Visualization of Liquid Reaction in Submerged Top-blow Agitation Process

Zhang, X.; Wu, J.; Zhang, H.; Ding, W.; Zhang, J.;

Originally published:

May 2020

Fuel Cells 21(2021)1, 18-23

DOI: https://doi.org/10.1002/fuce.202000016

Fuel Cells

Visualization of Liquid Reaction in Submerged Top-blow Agitation Process

Journal:	*Fuel Cells*
Manuscript ID	Draft
Wiley - Manuscript type:	Original Research Paper
Date Submitted by the Author:	n/a
Complete List of Authors:	Zhang, Xiao-hui wu, jiaying Zhang, han Ding, Wei Zhang, Jiayuan
Keywords:	Submerged top blow, Planar laser-induced fluorescence, Fluorescence quenching reaction, Liquid reaction process, Reaction degree

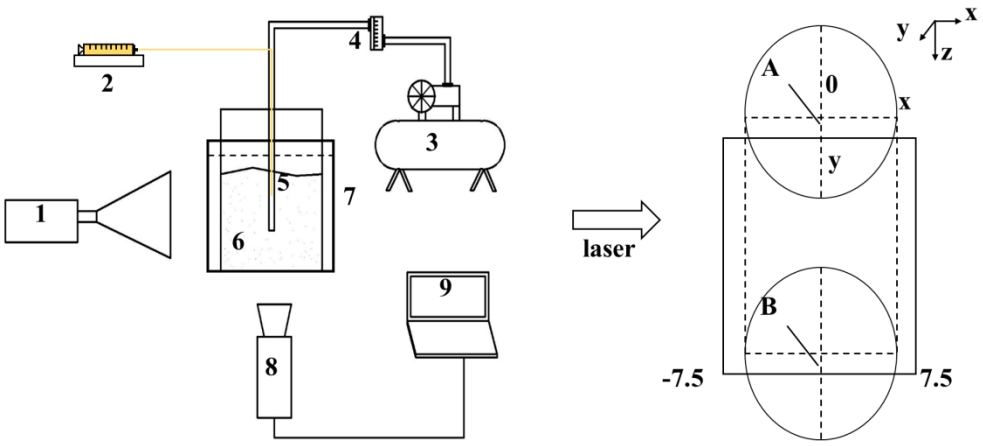

Fig. 1 Schematic of experimental system

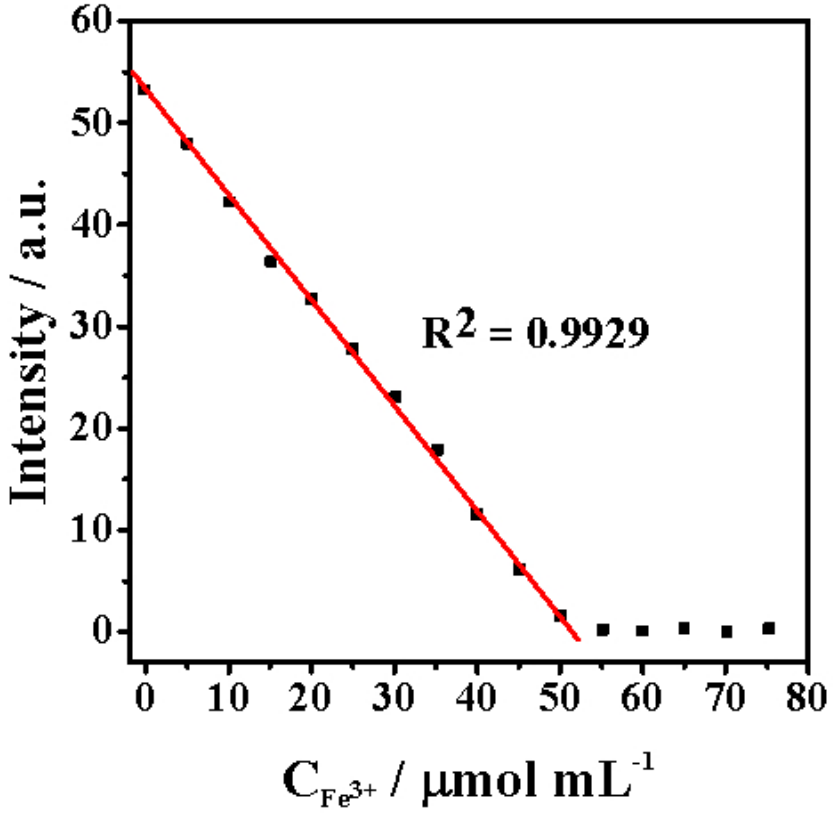

Fig. 2 Relationship between fluorescence intensity and Fe3+ concentration

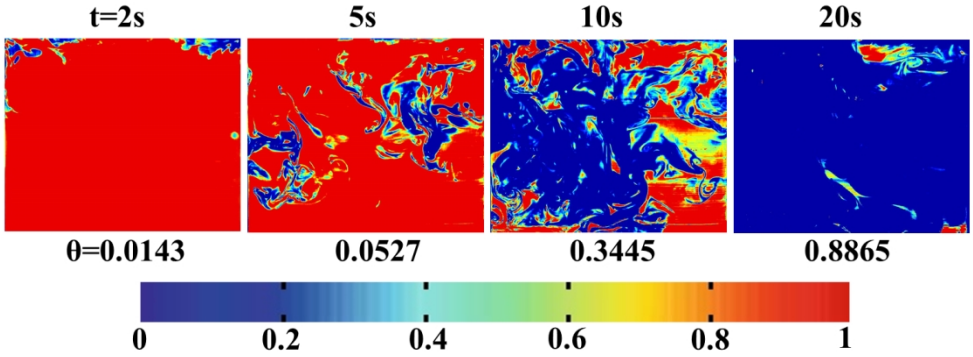

Fig. 3 Liquid reaction process

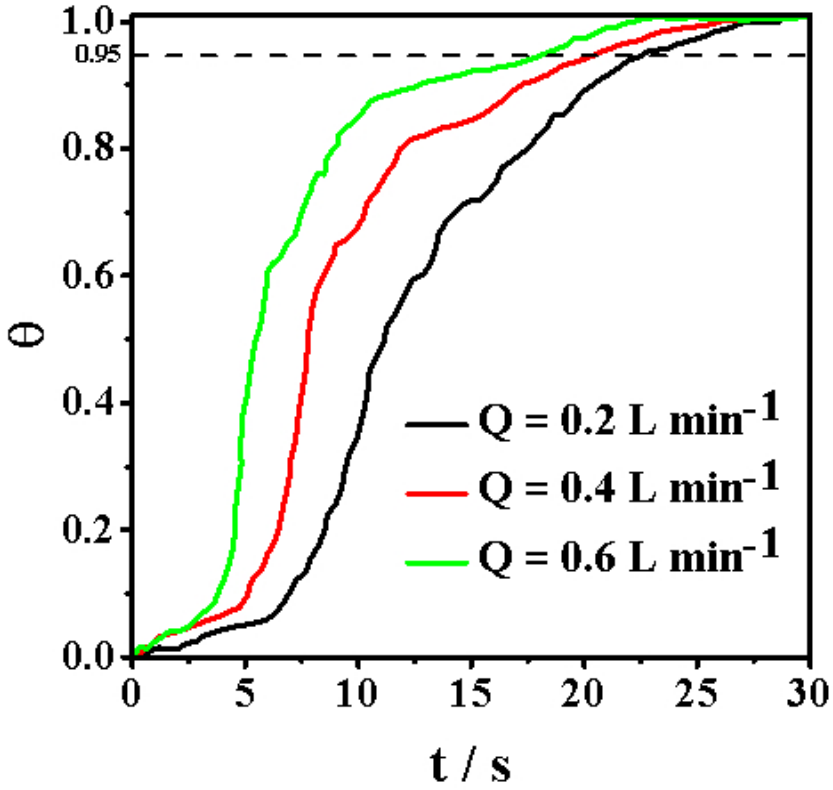

Fig. 4 Relationship between θ and t under different air flow rates

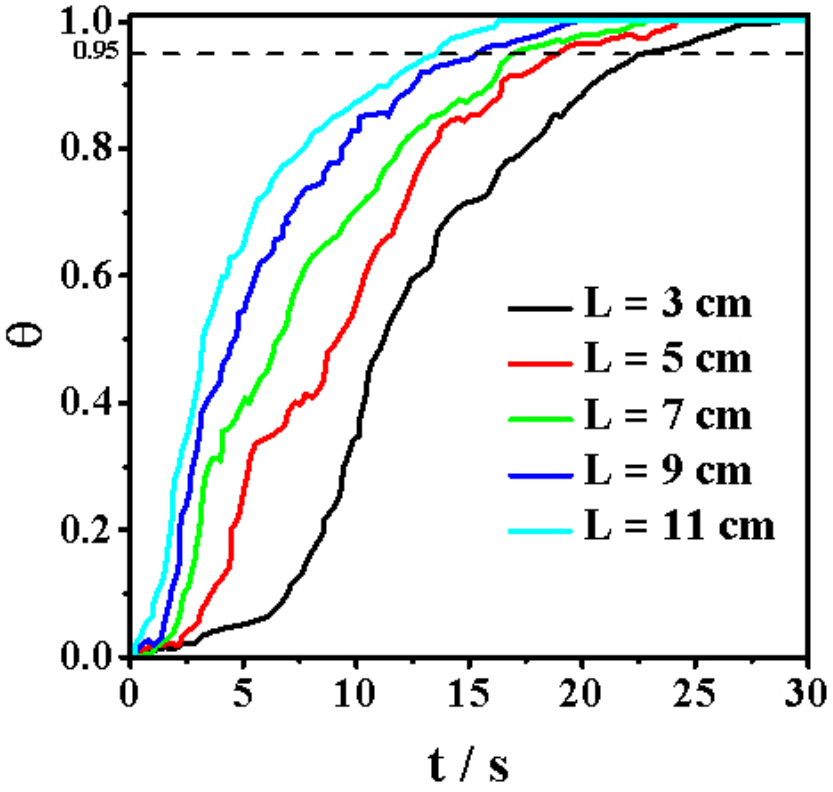

Fig. 5 Relationship between θ and t under different lance submerged depths of the spray gun

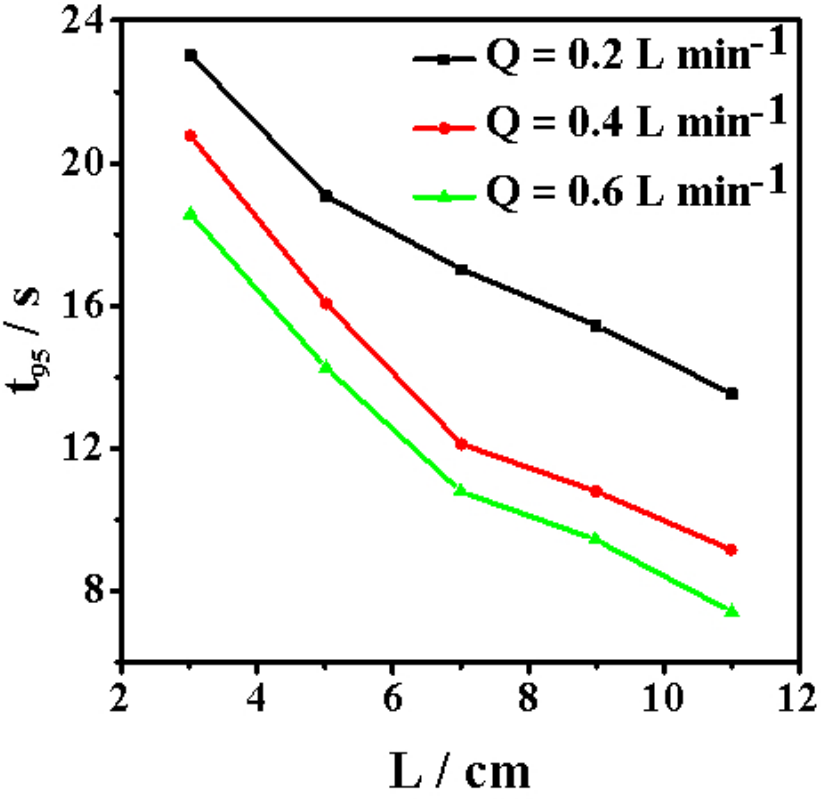

Fig. 6 Reaction time t95 for different lance submerged depths

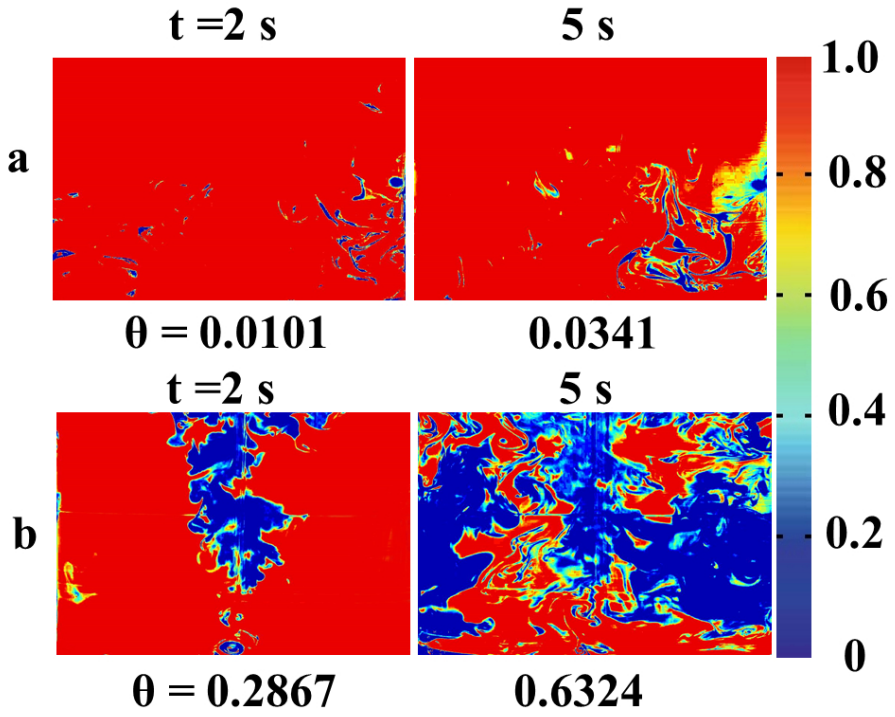

Fig. 7 Liquid reaction process for Fe3+ injection at point B

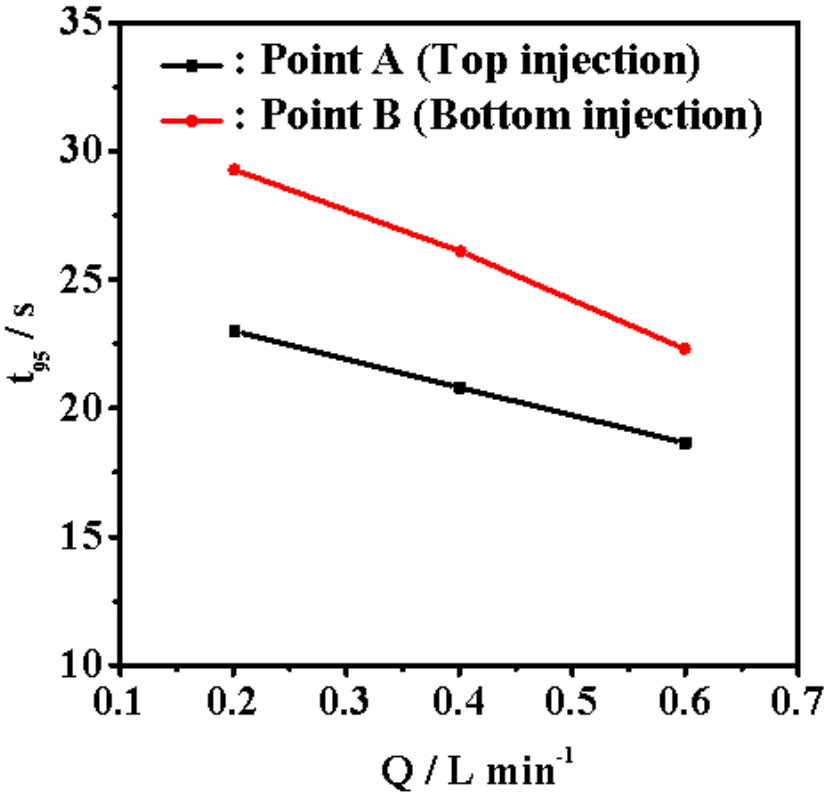

Fig. 8 Effect of air flow rate on reaction time t95 when Fe3+ is injected at points A and B respectively

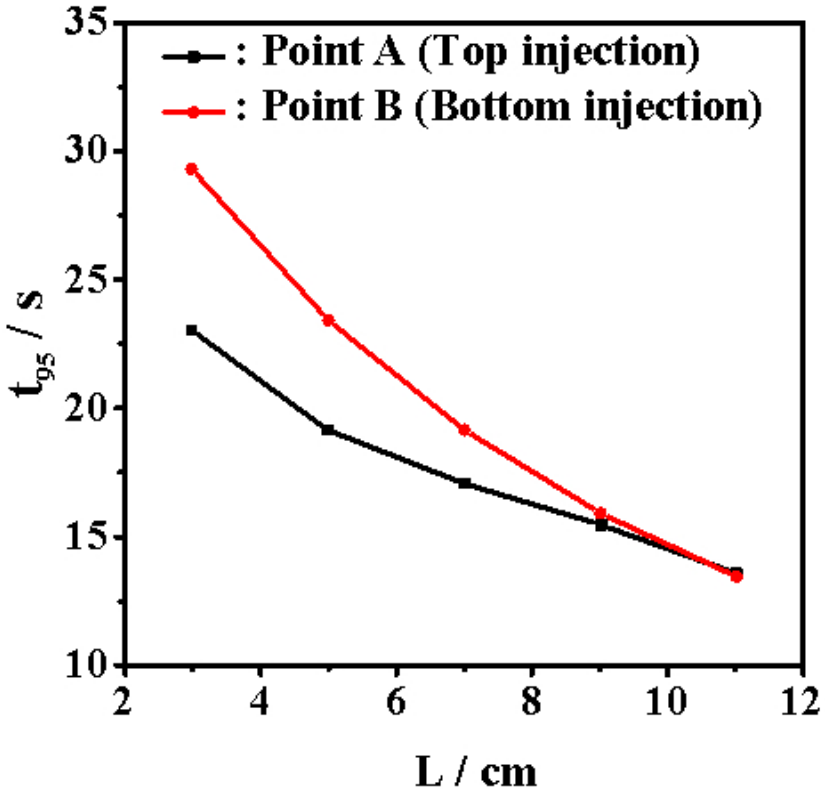

Fig. 9 Effect of lance submerged depth on reaction time t95 when Fe3+ is injected at point A and B

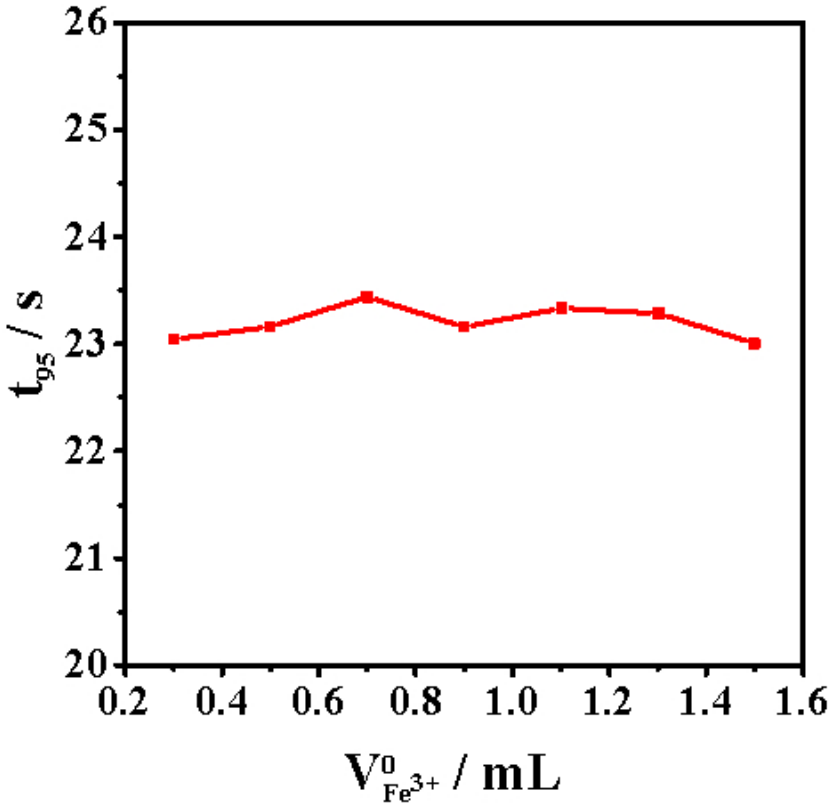

Fig. 10 Reaction time t95 under different initial volumes V0Fe3+

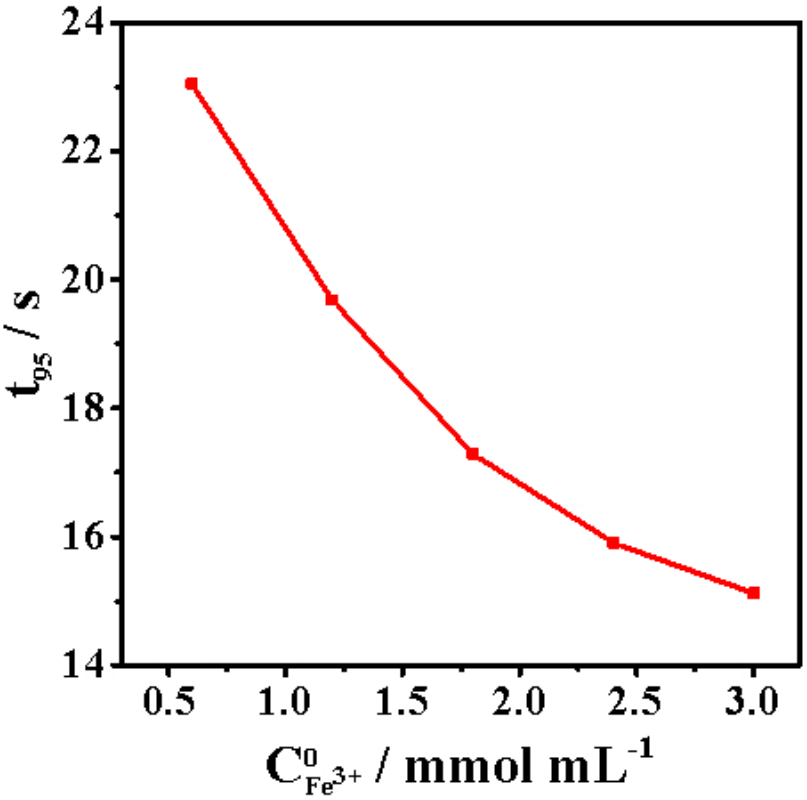

Fig. 11 Reaction time t95 under different initial concentrations C0Fe3+

Visualization of Liquid Reaction in Submerged Top-blow Agitation Process

Xiaohui Zhang[1], Jiaying Wu[1]*, Han Zhang[1,2], Wei Ding[3], Jiayuan Zhang[4]

[1]State Key Laboratory of Complex Nonferrous Metal Resources Clean Utilization, Kunming University of Science and Technology, Kunming, Yunnan 650093, China.

[2]Aluminum Corporation of China Limited Shandong Co., LTD, Zibo, Shandong 255052, PR China.

[3]Helmholtz-Zentrum Dresden-Rossendorf, Institute of Fluid Dynamics, 01328 Dresden, Germany.

[4]School of Energy Science and Engineering, Central South University, Changsha Hunan 410083, China.

Abstract

The liquid reaction in a submerged top-blow agitation process was studied using planar laser-induced fluorescence (PLIF) technology based on the principle of fluorescence quenching. The liquid reaction effects were analyzed using the reaction degree θ(t) and reaction time t_{95} under different conditions. The results show that the liquid reaction time decreases obviously for an increase in the air flow rate and submerged depth of the spray gun. The injection position of Fe^{3+} has a great influence on the reaction process; the reaction process is also different under other blowing conditions when Fe^{3+} is injected at the bottom. The reaction time of Fe^{3+} at the bottom injection position is higher than that at the top injection position; increasing the air flow rate and submerged depth of the spray gun can effectively reduce the difference in the reaction times at the two injection points. The effect of the injection position on

[*] Corresponding author, 1332529575@qq.com

the reaction time is eliminated when the spray gun submerged depth is close to the reactor bottom. The initial volume of Fe^{3+} has no obvious effect on the reaction time; however, an increase in the initial molarity of Fe^{3+} can decrease the reaction time.

Keywords: Fluorescence quenching reaction; Liquid reaction process; Planar laser-induced fluorescence; Reaction degree; Submerged top blow

1 Introduction

Submerged top-blows are widely used in chemical, metallurgical, industrial heating, and other industries [1-3]. After a bubble is generated from a nozzle, it rises to the liquid free surface due to the effect of buoyancy and drives the surrounding liquid to move, resulting in a complex gas-liquid two-phase flow phenomenon, accompanied by a complex multiphase reaction process [4-9].

At present, the research on submerged top-blow agitation is mainly focused on the velocity distribution of the gas-liquid phase flow field and the evaluation of the mixing effect. Using the LES and DPM models, Seong-Mook CHO et al. [4,5] researched the effect of submerged argon top-blowing and a magnetic field on the velocity and surface fluctuation of molten steel in the steelmaking process. YS Morsi et al. [6,7] simulated the velocity and temperature distribution of a melt liquid in the submerged jet agitation process. CA Llanos et al. [9-11] studied the flow field velocity means of numerical simulation, and compared and analyzed the results of the water distribution of gas and liquid in submerged bottom-blow and top-blow agitation bymodel experiment. Norifumi et al. [12-20] studied the factors which affect the mixing time in submerged top-blow, side-blow, and bottom-blow stirring agitation water model experiments, and the results showed that the air flow rate, depth of the molten pool, submerged depth, and diameter of the spray gun were the main factors. Less research has been done on the polyphase reaction process in submerged jet agitation [21-25]. N Huda et al. [21-23] researched the phase composition and reaction in the top-blow and side-blow process in zinc smelting, and simulated the

temperature and velocity changes in the molten pool based on the combustion model.

In recent years, planar laser-induced fluorescence (PLIF) has been widely used as a non-interference, visualized flow field measurement technology for the visualization and quantification of the concentration field [26,27], temperature field [28-30], and reaction process [31-34] in the liquid phase. In this research, PLIF technology was used to study the liquid phase reaction process in a submerged top-blow agitation reactor, and the characteristics of the liquid phase reaction in this reactor were revealed. The 2D visualization of the liquid phase reaction process was realized by detecting the changes in the fluorescence intensity after the reaction.

2 Experimental

As shown in Figure 1, the experiment system was composed of a planar laser, an injection pump, an air pump, a flowmeter, an air spray gun, a reactor, a high-speed camera, and a computer. The reactor was made of organic glass, and its inner diameter was 15.0cm. The liquid used was sodium fluorescein aqueous solution, and the liquid level height was 12.0cm. The inner and outer diameters of the air spray gun were 0.4 and 0.8cm, respectively. The air spray gun was located at the axes of the reactor and was vertically submerged in the liquid. The origin of the coordinates was the intersection of the reactor's axes and liquid surface. In order to avoid the irradiation of the air spray gun and bubbles by a laser plane, the laser plane and the reactor's axes were kept 2.0 cm (y = 2.0 cm) apart. The Fe^{3+} ($FeCl_3$) addition point was located at point A (x = 0,y= 1.0 cm,z = 0) of the liquid surface and point B (x = 0,y = 1.0 cm,z = 10.0 cm) of the liquid bottom. In order to avoid shooting interference due to light refraction and scattering, the reactor was placed in an organic glass tank which was filled with water.

Since the liquid produces a splashing phenomenon when the air flow rate is too high (when Q $\geqslant$ 1.0 L min^{-1}), the air flow rate was set as 0.2, 0.4, and 0.6 L min^{-1}(Q = 0.2, 0.4, and 0.6 L min^{-1}). The submerged depth of the spray gun was set as 3, 5, 7, 9,

and 11 cm(L = 3, 5, 7, 9, and 11 cm). Fe^{3+} was quickly added to the liquid(injection time was 0.5 s) using the injection pump after the experiment parameters were adjusted to the required values; the agitation time was set as 0(t = 0) at this moment, and the high-speed camera was used to record the fluorescence distribution on the laser plane continuously.

3 Results and Discussion

3.1 Quantitative Characterization Methods

A fluorescent agent emits fluorescence when irradiated by an excitation light; when some substances (such as Fe^{3+}, Cu^{2+}, and other metal ions) are added to a fluorescent agent, the fluorescent molecules react with these substances, causing the fluorescence to decrease or disappear. These substances can produce fluorescence quenching effects, and are called fluorescence quenchers [33]. In this study, Fe^{3+} ($FeCl_3$) was chosen as the fluorescence quencher for sodium fluorescein.

The fluorescein sodium concentration C_{Fl} was 0.5 μmol L^{-1} in the reactor 0.1 mL of Fe^{3+} ($C^0_{Fe}{}^{3+}$ = 0.1 mmol mL^{-1}) was added to the liquid fifteen times. As the volume of Fe^{3+} added (1.5 mL) was far lesser than that of the liquid (V_{liquid} = 2.0 L), the total volume was regarded as a constant. The camera recorded the fluorescence intensity after the mixing, and the measured data were used to calibrate the relationship between the fluorescence intensity and $C_{Fe}{}^{3+}$. As shown in Figure 2, the fluorescence intensity and $C_{Fe}{}^{3+}$ have a linear relationship when $C_{Fe}{}^{3+}$ = ~ 0-50 μmol L^{-1} ($C_{Fe}{}^{3+}/C_{Fl}$ = ~ 0-100). The fluorescence disappears completely and no longer changes when $C_{Fe}{}^{3+} \geq$ ~ 0-50 μmol L^{-1} ($C_{Fe}{}^{3+}/C_{Fl} \geq 100$).Therefore, unless otherwise specified, the initial concentration of Fe^{3+} was $C^0_{Fe}{}^{3+}$ = 0.6 mmol mL^{-1} and an initial volume is $V^0_{Fe}{}^{3+}$ = 0.3 mL was injected; therefore, $C_{Fe}{}^{3+}$ = 90 μmol L^{-1} in the reactor after the reaction, i.e., $C_{Fe}{}^{3+}/C_{Fl}$ = 180 after the reaction, ensuring a complete reaction.

$$\theta(t) = 1 - \frac{\sum_{n=1}^{Mx}\sum_{m=1}^{Mz} GV^*(x,z,t)}{\sum_{n=1}^{Mx}\sum_{m=1}^{Mz} GV^*(x,z,t_0)} \quad (1)$$

In order to quantitatively describe the reaction process, this paper introduces the concept of reaction degree [26]; the reaction degree on the measurement plane at time t is calculated as follows.

Where $\theta(t)$ is the statistical value of all the pixels at time t compared to the initial state at t_0; t_0 is the time when the tracer (fluorescein sodium) is injected; and $GV^*(x,z,t)$ and $GV^*(x,z,t_0)$ are the grey values of the position of a pixel point (x, z) after in situ calibration at time t and t_0, respectively. The $\theta(t)$ value was 0 before the reaction and 1 after the reaction completed. When the reaction degree is greater than 0.95 and is no longer less than 0.95 thereafter, the time taken is defined as the complete reaction time t_{95}.

3.2 Effect of Blow Characteristics on Reaction Process

A grayscale map is transformed into a pseudo color map by subtracting the background value, in order to facilitate observation. The pure blue part is the complete reaction area and the pure red part is the unreacted area.

Figure 3 shows the liquid reaction process at different times (L = 3 cm, Q = 0.2 L min^{-1}). When bubbles rise to the liquid free surface, they squeeze the nearby liquid and push it to both sides. Fe^{3+} also moves to both sides after it is added to the liquid; it then hits the reactor wall and moves downward. Fe^{3+} diffuses under the agitation of bubbles at the same time, and reacts with the fluorescent agent during the diffusion process and causes the fluorescence intensity to decrease or disappear. When the agitation time t = 20 s, the diffusion of Fe^{3+} is nearly complete under the constant agitation of the bubbles, and the fluorescence in the reactor almost completely disappears. When Fe^{3+} diffuses uniformly, the fluorescence disappears completely.

Figure 4 shows the relationship between θ and the agitation time *t* under different air flow rates (L = 3 cm). The Figure shows that the reaction process is divided into three stages. The first stage ($0 < \theta < 0.1$) is the beginning of the reaction process; Fe^{3+} has not been fully broken, and this makes the θ rise slowly in this stage. The second stage ($0.1 < \theta < 0.9$) is the interim of the reaction process; Fe^{3+} is spreading rapidly under the agitation of bubbles, and this makes the θ rise rapidly. The final stage ($0.9 < \theta < 1$) is the end of the reaction process; Fe^{3+} is fully dispersed, and the Fe^{3+} concentration tends to be constant in the reactor, and this makes the θ rise slowly and become stable. In addition, the Figure shows that the beginning stage become shorter as the air flow rate increases. The greater the air flow rate, the higher the θ under the same stir time in the interim stage. The reaction time t_{95} decreases as the air flow rate increases, because the higher flow rate makes the agitation more intense,resulting in a more quick reaction.

Figure 5 is the plot of θ vs stir time *t* under different air lance submerged depths of the spray gun (Q = 0.2 L min^{-1}). The Figure shows that at a greater depth, the θ rises faster. The liquid is fully stirred when the lance is moved towards the bottom of the liquid (L = 9, 11 cm);Fe^{3+} is quickly broken and spread. The reaction time t_{95} decreases as the spray gun submerged depth increase. This is because the deeper submergence can increase the rise time of the bubbles; the agitation of the liquid is intensified, and this promotes the progress of the reaction.

Figure 6 shows the reaction time t_{95} for different submerged depths of the spray gun. As shown, the reaction time t_{95} decreases for a higher submerged depth under the same air flow rate. The minimum reaction time t_{95} is 13.56 s at L = 11 cm and the maximum reaction time t_{95} is 23.04 s at L = 3 cm when Q = 0.2 L min^{-1}. In addition, the reaction time t_{95} decreases as the air flow rate increases when the lance submerged depth remains unchanged.

3.3 Effect of Fe^{3+} Injection Point on Reaction Process

Figure 7 shows the reaction process of Fe^{3+} injection at bottom point B. As shown in the Figure, the reaction processes were quite different under various conditions when the Fe^{3+} injection point was at the bottom. When the submerged depth of the air lance is relatively shallow (L = 3 cm), the liquid at the bottom is difficult to fully stir using bubbles; the fluidity is poor, which makes it difficult for Fe^{3+} to diffuse after injection at point B, and greatly increases the reaction time. When L = 3 cm, the reaction time of injection at point B (29.32 s) is much longer than that at point A (23.04 s). When the spray gun is close to the bottom of the reactor (L = 11 cm), the bottom of the liquid phase is fully agitated by bubbles, and Fe^{3+} is rapidly brought to the upper layer of the liquid by bubbles after injection at point B; thus, Fe^{3+} is fully diffused. When L = 11 cm, the reaction time of injection at point B (13.42 s) is nearly consistent with that at point A (13.5 s).

Figure 8 shows the influence of the Fe^{3+} injection location on the reaction time for different air flow rates. The Figure shows that Fe^{3+} injection at either the top point A or bottom point B can reduce the reaction time by increasing the air flow rate. However, the reaction time of Fe^{3+} injection at the bottom point B is much longer than that at the top point A for the same air flow rate. The reaction times of injection at point B are 27.3%, 25.7%, and 19.7% higher than those at point A when Q = 0.2, 0.4, and 0.6 L min^{-1}, respectively. This indicates that an increase in the air flow rate can reduce the influence of the injection location on the reaction time. This is because an increase in the air flow rate results in effective agitation of the liquid at the bottom of the reactor and reduces the flow difference of the reactor.

Figure 9 shows the influence of the injection point location on the reaction time for different submerged depths of the air lance. The Figure shows that when Fe^{3+} is injected at point A or point B, an increase in the submerged depth can reduce the reaction time. The greater the submerged depth of the air lance, the smaller the difference between the reaction times of Fe^{3+} injection at A and B. The reaction time of injection at the bottom point B are 27.3%, 22.7%, and 12.2% higher than those at the top point A when L = 3, 5, and 7 cm, respectively. The reaction time of injection

at point B is consistent with that at point A when L = 9 and 11 cm, indicating that an increase in the submerged depth can reduce the influence of the injection point position on the reaction time. When the submerged depth is close to the bottom of the reactor, the influence of the injection point location on the reaction time is eliminated. This is because an increase in the submerged depth results in effective agitation of the liquid at the bottom of the reactor, and reduces the flow difference of the reactor. When the submerged depth is close to the bottom of the reactor, the liquid in the bottom is fully agitated by bubbles; therefore, the influence of the injection point location on the reaction time is eliminated.

Figure 10 shows the influence of the Fe^{3+} initial volume $V^0_{Fe^{3+}}$ on the reaction time. The $V^0_{Fe^{3+}}$ was set as 0.3, 0.5, 0.7, 0.9, 1.1, 1.3, and 1.5 mL, whereas the total amount of Fe^{3+} (nFe^{3+}) was 1.8×10^{-4} mol, making $C_{Fe^{3+}}$ 90 mol L^{-1}, i.e., $C_{Fe^{3+}}/C_{Fl}$ was 180 for each reaction. The injection time was 0.5 s. $V^0_{Fe^{3+}}$ had little influence on the reaction time. The average reaction time was 23.19 s, and the maximum value was only 2.0% higher than the minimum. Although an increase in $V^0_{Fe^{3+}}$ had a diffusion effect on Fe^{3+}, it was still far less than that of liquid volume (V_{liquid} = 2.0 L), and the diffusion effect could be ignored relative to the agitation effect of the bubbles.

3.4 Effects of Initial Volume of Fe^{3+} ($V^0_{Fe^{3+}}$) and Initial Concentration of Fe^{3+} ($C^0_{Fe^{3+}}$) on Reaction Time

Figure 11 shows the influence of the Fe^{3+} initial concentration $C^0_{Fe^{3+}}$ on the reaction time. The $C^0_{Fe^{3+}}$ was set as 0.6, 1.2, 1.8, 2.4, and 3.0 mmol mL^{-1}, whereas the $V^0_{Fe^{3+}}$ was 0.3 mL, i.e., $C_{Fe^{3+}}/C_{Fl}$ was 180, 360, 540, 720, and 900, respectively. As shown in Figure 11,the $C^0_{Fe^{3+}}$ has a great influence on the reaction time. The larger the $C^0_{Fe^{3+}}$, the shorter the reaction time. This is because a larger $C^0_{Fe^{3+}}$ results in a higher the concentration of Fe^{3+} in the molecular groups formed in the diffusion process, and a stronger quenching effect on the fluorescence such that the reaction time is greatly reduced. In addition, the Figure shows that for a larger $C^0_{Fe^{3+}}$ is, the difference between the reaction times for the two adjacent points is smaller.

4 Conclusions

(i)The planar laser-induced fluorescence technique was used to measure the two-dimensional distribution of the liquid phase reaction in submerged top-blow agitation. The reaction process of the liquid phase shown an obvious difference under different agitation conditions.

(ii)When the submerged depth is relatively shallow, the fluidity at the bottom of the reactor is poor, and the fluorescence quenching agent (Fe^{3+}) is difficult to diffuse after injection at the bottom, making the reaction time much longer than that at the top. Increasing the air flow rate and the submerged depth can improve the fluidity at the bottom so that Fe^{3+} can be fully diffused after injection at the bottom, and the reaction time gap between the two injection points can be narrowed. When the submerged depth is close to the bottom of the reactor, the reaction times for the two injection points tend to be consistent.

(iii)In the experiment, the initial volume of Fe^{3+} is much smaller than that of the fluorescent solution. Therefore, a change in the initial volume of Fe^{3+} has no significant effect on the reaction time; the higher the initial concentration of Fe^{3+}, the shorter the reaction time.

Acknowledgement

We are grateful to the support provided by the Natural Science Foundation of China (No. U1602272) for this research. We are also grateful to Dr. Yixiang Liao in Helmholtz-Zentrum Dresden-Rossendorf for providing her feedback and discussing the research.

References

[1] I. El-Katatny, Y.S. Morsi, W. Yang, *Ironmak. Steelmak.* **2008**, 2, 91.

[2] J. Hoang, M.A. Reuter, R. Matusewicz, S. Hughes, N. Piret, *Miner. Eng.*

2008, 9,742.

[3] C. Qi, W. Wang, B. Wang, Y. Kuang, J. Xu, *J. Nat. Gas. Sci. Eng.* 2016, 31, 313.

[4] S.M. Cho, S.H. Kim, B.G. Thomas, *Isij. Int.* **2015**, 4, 845.

[5] S.M. Cho, S.H. Kim, B.G. Thomas, *Trans. Isij.* **2014**, 4, 855.

[6] Y.S. Morsi, W. Yang, I. El-Katatny, *Ironmak. Steelmak.* **2008**, 1,69.

[7] J.Q. Zhang, N.J. Zhou, S.H. Zhou, *J. Cent. South. Univ.* **2011**, 5,1726.

[8] Q.T. Xiao, K. Yang, M.M. Wu, J.X. Pan, J.X. Xu, H. Wang, *Appl. Therm. Eng.* **2018**, 138, 832.

[9] C.A. Llanos, G. Saul, R. J. Angel, J. d. J. Barreto, S. Gildardo, *Isij. Int.* **2010**, 3, 396.

[10] Y.S. Morsi, W. Yang, D. Achim, A. Acquadro, *J. Aging. Phys. Activ.* **2001**, 4, 247.

[11] K.S. Lee, W.O. Yang, Y.G. Park, K.W. Yi, Metals & Materials **2000**, 5, 461.

[12] N. Kochi, K. Mori, Y. Sasaki, M. Iguchi, *Isij. Int.* **2011**, 3,344.

[13] H. Zhao, L. Zhang, P. Yin, S. Wang, *Int. J. Chem. React. Eng.* **2017**, 3.

[14] Y. S. Morsi, W. Yang, B.R. Clayton, N.B. Gray, *Can. Metall. Quart.* **2000**, 1, 87.

[15] A. Nordquist, N. Kumbhat, L. Jonsson, P. Jönsson, *Steel. Res. Int.* **2010**, 2, 82.

[16] M. Ramã-Rez-Argã¡Ez, *Adv. Mater. Process.* **2007**, 1, 59.

[17] P. Ternstedt, A. Tilliander, P.G. Jonsson, M. Iguchi, *Isij. Int.* **2010**, 5, 663.

[18] Y. Li, W.T. Lou, M.Y. Zhu, *Ironmak. Steelmak.* **2013**, 7, 505.

[19] L. Shui, Z. Cui, X. Ma, M.A. Rhamdhani, A. Nguyen, B. Zhao, *Metall. Mater. Trans. B.* **2015**, 3, 1218.

[20] N. Huda, J. Naser, G. Brooks, M.A. Reuter, *Lecture Notes in Engineering & Computer Science* **2010**, 1, 39.

[21] N. Huda, J. Naser, G. Brooks, M.A. Reuter, R.W. Matusewicz, *Metall. Mater. Trans. B.* **2011**, 1, 39.

[22] N. Huda, J. Naser, G. Brooks, M.A. Reuter, R.W. Matusewicz, *Metall. Mater. Trans. B.* **2012**, 5, 1054.

[23] M.A. Sattar, J. Naser, G. Brooks, Procedia Engineering **2013**, 56, 421.

[24] K. Byung-Su, J. Soo-Buck, L. Jae-Chun, D. Shin, M. Nam-Il, *Mater. Trans.* **2012**, 5, 985.

[25] L.A. Torres, B.A. Fleck, D.J. Wilson, D.S. Nobes, *Measurement* **2013**, 8, 2597.

[26] M.X. Zhang, Y.Y. Hu, W.T. Wang, T. Shao, Y. Cheng, *Chem. Eng. Process.* **2013**, 4, 36.

[27] A. Asthana, I. Zinovik, C. Weinmueller, D. Poulikakos, *Int. J. Heat. Mass. Tran.* **2011**, 7, 1456.

[28] M. Bruchhausen, F. Guillard, F. Lemoine, *Exp. Fluids.* **2005**, 1, 123.

[29] S.V. Roman, A.S. *Appl. Therm. Eng.* **2017**, 127, 141.

[30] Y.Y. Hu, Z. Liu, J.C. Yang, Y. Jin, Y. Cheng, *Chem. Eng. Sci.* **2010**, 15, 4511.

[31] A. Lehwald, D. Thévenin, K. Zähringer, *Exp. Fluids.* **2010**, 5, 823.

[32] V. Zhdanov, A. Chorny, *Int. J. Heat. Mass. Tran.* **2011**, 15, 3245.

[33] I. Sancho, S. Varela, A. Vernet, J. Pallares, *Int. J. Heat. Mass. Tran.* **2016**, 93, 155.

[34] M.R. Eftink, *Springer US* **2001**, 2, 53.

Figure Captions:

Fig. 1 Schematic of experimental system:1-laser, 2-injection pump(Fe^{3+}), 3-air pump, 4-flowmeter, 5-air spray gun, 6-reactor (Fl) , 7-square glass tank, 8-high-speed camera, 9-computer.

Fig. 2 Relationship between fluorescence intensity and Fe^{3+} concentration.

Fig. 3 Liquid reaction process(L = 3 cm, Q = 0.2 L min^{-1}; Injection point is A).

Fig. 4 Relationship between θ and *t* under different air flow rates(L = 3 cm; Injection point is at A).

Fig. 5 Relationship between θ and *t* under different lance submerged depths of the spray gun(Q = 0.2 L min^{-1}; Injection point is at A).

Fig. 6 Reaction time t_{95} for different lance submerged depths(Injection point is at A).

Fig. 7 Liquid reaction process for Fe^{3+} injection at point B(Q = 0.2 L min^{-1}; a: L = 3 cm, b: L = 11 cm).

Fig. 8 Effect of air flow rate on reaction time t_{95} when Fe^{3+} is injected at points A and B respectively (L = 3 cm).

Fig. 9 Effect of lance submerged depth on reaction time t_{95} when Fe^{3+} is injected at point A and B (Q = 0.2 L min^{-1}).

Fig. 10 Reaction time t_{95} under different initial volumes $V^0_{Fe^{3+}}$(L = 3 cm, Q= 0.2 L min^{-1}; Injection point is at A).

Fig. 11 Reaction time t_{95} under different initial concentrations $C^0_{Fe^{3+}}$ (L = 3 cm, Q = 0.2 L min^{-1}; Injection point is A).